Research Article | Vol. 8, No. 8 | 1 Aug 2017 | BIOMEDICAL OPTICS EXPRESS 3700
Biomedical Optics EXPRESS

Label-free optical detection of action potential in mammalian neurons

SUBRATA BATABYAL,[1,3,6,7] SARMISHTHA SATPATHY,[2,6] LOAN BUI,[3] YOUNG-TAE KIM,[3] SAMARENDRA MOHANTY,[1] ROBERT BACHOO,[4] AND DIGANT P. DAVÉ[3,5,8]

[1]*Nanoscope Technologies, Arlington, TX, USA*
[2]*Department of Electrical Engineering, University of Texas at Arlington, TX, USA*
[3]*Department of Bioengineering, University of Texas at Arlington, TX, USA*
[4]*Department of Neurology and Neurotherapeutics, University of Texas Southwestern Medical Center, Dallas, TX, USA*
[5]*Advance Imaging Research Centre, University of Texas Southwestern Medical Center, Dallas, TX, USA*
[6]*Equal Contribution*
[7]*sbatabyal@nanoscopetech.com*
[8]*ddave@uta.edu*

Abstract: We describe an optical technique for label-free detection of the action potential in cultured mammalian neurons. Induced morphological changes due to action potential propagation in neurons are optically interrogated with a phase sensitive interferometric technique. Optical recordings composed of signal pulses mirror the electrical spike train activity of individual neurons in a network. The optical pulses are transient nanoscale oscillatory changes in the optical path length of varying peak magnitude and temporal width. Exogenous application of glutamate to cortical neuronal cultures produced coincident increase in the electrical and optical activity; both were blocked by application of a Na-channel blocker, Tetrodotoxin. The observed transient change in optical path length in a single optical pulse is primarily due to physical fluctuations of the neuronal cell membrane mediated by a yet unknown electromechanical transduction phenomenon. Our analysis suggests a traveling surface wave in the neuronal cell membrane is responsible for the measured optical signal pulses.

OCIS codes: (120.3180) Interferometry; (120.5050) Phase measurement; (170.2655) Functional monitoring and imaging; (180.3170) Interference microscopy; (120.5820) Scattering measurements.

References and links

1. R. Q. Quiroga, L. Reddy, G. Kreiman, C. Koch, and I. Fried, "Invariant visual representation by single neurons in the human brain," Nature **435**(7045), 1102–1107 (2005).
2. G. Rees, G. Kreiman, and C. Koch, "Neural correlates of consciousness in humans," Nat. Rev. Neurosci. **3**(4), 261–270 (2002).
3. D. S. Bassett and E. T. Bullmore, "Human brain networks in health and disease," Curr. Opin. Neurol. **22**(4), 340–347 (2009).
4. C. Lossin, T. H. Rhodes, R. R. Desai, C. G. Vanoye, D. Wang, S. Carniciu, O. Devinsky, and A. L. George, Jr., "Epilepsy-associated dysfunction in the voltage-gated neuronal sodium channel scn1a," J. Neurosci. **23**(36), 11289–11295 (2003).
5. J. K. Mueller and W. J. Tyler, "A quantitative overview of biophysical forces impinging on neural function," Phys. Biol. **11**(5), 051001 (2014).
6. B. Sakmann and E. Neher, "Patch clamp techniques for studying ionic channels in excitable membranes," Annu. Rev. Physiol. **46**(1), 455–472 (1984).
7. F. J. Sigworth and E. Neher, "Single na+ channel currents observed in cultured rat muscle cells," Nature **287**(5781), 447–449 (1980).
8. M. Scanziani and M. Häusser, "Electrophysiology in the age of light," Nature **461**(7266), 930–939 (2009).
9. A. K. Engel, C. K. E. Moll, I. Fried, and G. A. Ojemann, "Invasive recordings from the human brain: Clinical insights and beyond," Nat. Rev. Neurosci. **6**(1), 35–47 (2005).
10. J. Dunlop, M. Bowlby, R. Peri, D. Vasilyev, and R. Arias, "High-throughput electrophysiology: An emerging paradigm for ion-channel screening and physiology," Nat. Rev. Drug Discov. **7**(4), 358–368 (2008).

#291857 https://doi.org/10.1364/BOE.8.003700
Journal © 2017 Received 4 Apr 2017; revised 26 Jun 2017; accepted 27 Jun 2017; published 19 Jul 2017
Corrected: 25 July 2017

Biomedical Optics EXPRESS

11. M. E. Spira and A. Hai, "Multi-electrode array technologies for neuroscience and cardiology," Nat. Nanotechnol. **8**(2), 83–94 (2013).
12. X. Li, W. Zhou, M. Liu, and Q. Luo, "Synchronized spontaneous spikes on multi-electrode array show development of cultured neuronal network," Conf. Proc. IEEE Eng. Med. Biol. Soc. **2**, 2134–2137 (2005).
13. B. Eversmann, M. Jenkner, F. Hofmann, C. Paulus, R. Brederlow, B. Holzapfl, P. Fromherz, M. Merz, M. Brenner, M. Schreiter, R. Gabl, K. Plehnert, M. Steinhauser, G. Eckstein, D. Schmitt-Landsiedel, and R. Thewes, "A 128x128 cmos biosensor array for extracellular recording of neural activity," Ieee J Solid-St Circ **38**(12), 2306–2317 (2003).
14. L. B. Cohen, "Changes in neuron structure during action potential propagation and synaptic transmission," Physiol. Rev. **53**(2), 373–418 (1973).
15. W. N. Ross, B. M. Salzberg, L. B. Cohen, A. Grinvald, H. V. Davila, A. S. Waggoner, and C. H. Wang, "Changes in absorption, fluorescence, dichroism, and birefringence in stained giant axons: optical measurement of membrane potential," J. Membr. Biol. **33**(1), 141–183 (1977).
16. L. B. Cohen and B. M. Salzberg, "Optical measurement of membrane potential," Rev. Physiol. Biochem. Pharmacol. **83**, 35–88 (1978).
17. L. Jin, Z. Han, J. Platisa, J. R. A. Wooltorton, L. B. Cohen, and V. A. Pieribone, "Single action potentials and subthreshold electrical events imaged in neurons with a fluorescent protein voltage probe," Neuron **75**(5), 779–785 (2012).
18. D. S. Peterka, H. Takahashi, and R. Yuste, "Imaging voltage in neurons," Neuron **69**(1), 9–21 (2011).
19. C. Grienberger and A. Konnerth, "Imaging calcium in neurons," Neuron **73**(5), 862–885 (2012).
20. L. Tian, S. A. Hires, and L. L. Looger, "Imaging neuronal activity with genetically encoded calcium indicators," Cold Spring Harb. Protoc. **2012**(6), 647–656 (2012).
21. S. Reichinnek, A. von Kameke, A. M. Hagenston, E. Freitag, F. C. Roth, H. Bading, M. T. Hasan, A. Draguhn, and M. Both, "Reliable optical detection of coherent neuronal activity in fast oscillating networks in vitro," Neuroimage **60**(1), 139–152 (2012).
22. S. Berlin, E. C. Carroll, Z. L. Newman, H. O. Okada, C. M. Quinn, B. Kallman, N. C. Rockwell, S. S. Martin, J. C. Lagarias, and E. Y. Isacoff, "Photoactivatable genetically encoded calcium indicators for targeted neuronal imaging," Nat. Methods **12**(9), 852–858 (2015).
23. F. St-Pierre, M. Chavarha, and M. Z. Lin, "Designs and sensing mechanisms of genetically encoded fluorescent voltage indicators," Curr. Opin. Chem. Biol. **27**, 31–38 (2015).
24. S. Inagaki and T. Nagai, "Current progress in genetically encoded voltage indicators for neural activity recording," Curr. Opin. Chem. Biol. **33**, 95–100 (2016).
25. J. Bradley, R. Luo, T. S. Otis, and D. A. DiGregorio, "Submillisecond optical reporting of membrane potential in situ using a neuronal tracer dye," J. Neurosci. **29**(29), 9197–9209 (2009).
26. C. B. Chien and J. Pine, "Voltage-sensitive dye recording of action potentials and synaptic potentials from sympathetic microcultures," Biophys. J. **60**(3), 697–711 (1991).
27. C. Wolff, B. Fuks, and P. Chatelain, "Comparative study of membrane potential-sensitive fluorescent probes and their use in ion channel screening assays," J. Biomol. Screen. **8**(5), 533–543 (2003).
28. D. R. Hochbaum, Y. Zhao, S. L. Farhi, N. Klapoetke, C. A. Werley, V. Kapoor, P. Zou, J. M. Kralj, D. Maclaurin, N. Smedemark-Margulies, J. L. Saulnier, G. L. Boulting, C. Straub, Y. K. Cho, M. Melkonian, G. K. S. Wong, D. J. Harrison, V. N. Murthy, B. L. Sabatini, E. S. Boyden, R. E. Campbell, and A. E. Cohen, "All-optical electrophysiology in mammalian neurons using engineered microbial rhodopsins," Nat. Methods **11**(8), 825–833 (2014).
29. J. M. Kralj, A. D. Douglass, D. R. Hochbaum, D. Maclaurin, and A. E. Cohen, "Optical recording of action potentials in mammalian neurons using a microbial rhodopsin," Nat. Methods **9**(1), 90–95 (2011).
30. G. Cao, J. Platisa, V. A. Pieribone, D. Raccuglia, M. Kunst, and M. N. Nitabach, "Genetically targeted optical electrophysiology in intact neural circuits," Cell **154**(4), 904–913 (2013).
31. R. A. Stepnoski, A. LaPorta, F. Raccuia-Behling, G. E. Blonder, R. E. Slusher, and D. Kleinfeld, "Noninvasive detection of changes in membrane potential in cultured neurons by light scattering," Proc. Natl. Acad. Sci. U.S.A. **88**(21), 9382–9386 (1991).
32. A. J. Foust and D. M. Rector, "Optically teasing apart neural swelling and depolarization," Neuroscience **145**(3), 887–899 (2007).
33. B. W. Graf, T. S. Ralston, H. J. Ko, and S. A. Boppart, "Detecting intrinsic scattering changes correlated to neuron action potentials using optical coherence imaging," Opt. Express **17**(16), 13447–13457 (2009).
34. J. L. Schei, M. D. McCluskey, A. J. Foust, X. C. Yao, and D. M. Rector, "Action potential propagation imaged with high temporal resolution near-infrared video microscopy and polarized light," Neuroimage **40**(3), 1034–1043 (2008).
35. A. H. Badreddine, T. Jordan, and I. J. Bigio, "Real-time imaging of action potentials in nerves using changes in birefringence," Biomed. Opt. Express **7**(5), 1966–1973 (2016).
36. T. Akkin, D. Davé, T. Milner, and H. Rylander Iii, "Detection of neural activity using phase-sensitive optical low-coherence reflectometry," Opt. Express **12**(11), 2377–2386 (2004).
37. C. Fang-Yen, M. C. Chu, H. S. Seung, R. R. Dasari, and M. S. Feld, "Noncontact measurement of nerve displacement during action potential with a dual-beam low-coherence interferometer," Opt. Lett. **29**(17), 2028–2030 (2004).

Biomedical Optics EXPRESS

38. M. A. Choma, A. K. Ellerbee, C. Yang, T. L. Creazzo, and J. A. Izatt, "Spectral-domain phase microscopy," Opt. Lett. **30**(10), 1162–1164 (2005).
39. L. B. Cohen, B. Hille, and R. D. Keynes, "Changes in axon birefringence during the action potential," J. Physiol. **211**(2), 495–515 (1970).
40. D. Hill and R. Keynes, "Opacity changes in stimulated nerve," J. Physiol. **108**(3), 278–281 (1949).
41. C. Fang-Yen and M. S. Feld, "Intrinsic optical signals in neural tissues: Measurements, mechanisms, and applications," Acs Sym. Ser. **963**, 219–235 (2007).
42. M. Q. Tong, M. M. Hasan, S. S. Lee, M. R. Haque, D. H. Kim, M. S. Islam, M. E. Adams, and B. H. Park, "OCT intensity and phase fluctuations correlated with activity-dependent neuronal calcium dynamics in the drosophila CNS [Invited]," Biomed. Opt. Express **8**(2), 726–735 (2017).
43. T. Akkin, D. Landowne, and A. Sivaprakasam, "Optical coherence tomography phase measurement of transient changes in squid giant axons during activity," J. Membr. Biol. **231**(1), 35–46 (2009).
44. Y. J. Yeh, A. J. Black, D. Landowne, and T. Akkin, "Optical coherence tomography for cross-sectional imaging of neural activity," Neurophotonics **2**(3), 035001 (2015).
45. T. Akkin, C. Joo, and J. F. de Boer, "Depth-resolved measurement of transient structural changes during action potential propagation," Biophys. J. **93**(4), 1347–1353 (2007).
46. G. H. Kim, P. Kosterin, A. L. Obaid, and B. M. Salzberg, "A mechanical spike accompanies the action potential in mammalian nerve terminals," Biophys. J. **92**(9), 3122–3129 (2007).
47. B. M. Salzberg, A. L. Obaid, and H. Gainer, "Large and rapid changes in light scattering accompany secretion by nerve terminals in the mammalian neurohypophysis," J. Gen. Physiol. **86**(3), 395–411 (1985).
48. S. Oh, C. Fang-Yen, W. Choi, Z. Yaqoob, D. Fu, Y. Park, R. R. Dassari, and M. S. Feld, "Label-free imaging of membrane potential using membrane electromotility," Biophys. J. **103**(1), 11–18 (2012).
49. L. Mandel and E. Wolf, "Optical Coherence and Quantum Optics*" p173* (Cambrige University Press, 1995).
50. C. Joo, T. Akkin, B. Cense, B. H. Park, and J. F. de Boer, "Spectral-domain optical coherence phase microscopy for quantitative phase-contrast imaging," Opt. Lett. **30**(16), 2131–2133 (2005).
51. T. Narahashi, J. W. Moore, and W. R. Scott, "Tetrodotoxin blockage of sodium conductance increase in lobster giant axons," J. Gen. Physiol. **47**(5), 965–974 (1964).
52. K. Iwasa and I. Tasaki, "Mechanical changes in squid giant axons associated with production of action potentials," Biochem. Biophys. Res. Commun. **95**(3), 1328–1331 (1980).
53. A. El Hady and B. B. Machta, "Mechanical surface waves accompany action potential propagation," Nat. Commun. **6**, 6697 (2015).
54. T. Heimburg and A. D. Jackson, "On the action potential as a propagating density pulse and the role of anesthetics," Biophys. Rev. Lett. **2**(01), 57–78 (2007).
55. I. Tasaki and P. M. Byrne, "Volume expansion of nonmyelinated nerve fibers during impulse conduction," Biophys. J. **57**(3), 633–635 (1990).
56. E. Sassaroli and N. Vykhodtseva, "Acoustic neuromodulation from a basic science prospective," J. Ther. Ultrasound **4**(1), 17 (2016).
57. D. Gross, W. S. Williams, and J. A. Connor, "Theory of electromechanical effects in nerve," Cell. Mol. Neurobiol. **3**(2), 89–111 (1983).
58. R. Budvytyte, A. Gonzalez-Perezl, L. D. Mosgaard, E. Villagran-Vargas, A. D. Jackson, and T. Heimburg, "Solitary electromechanical pulses in lobster neurons," Biophys. J. **110**(3), 150a (2016).
59. P. C. Zhang, A. M. Keleshian, and F. Sachs, "Voltage-induced membrane movement," Nature **413**(6854), 428–432 (2001).
60. S. Shrivastava and M. F. Schneider, "Evidence for two-dimensional solitary sound waves in a lipid controlled interface and its implications for biological signalling," J. R. Soc. Interface **11**(97), 20140098 (2014).
61. A. E. Pelling, S. Sehati, E. B. Gralla, J. S. Valentine, and J. K. Gimzewski, "Local nanomechanical motion of the cell wall of saccharomyces cerevisiae," Science **305**(5687), 1147–1150 (2004).
62. J. Griesbauer, S. Bössinger, A. Wixforth, and M. F. Schneider, "Propagation of 2d pressure pulses in lipid monolayers and its possible implications for biology," Phys. Rev. Lett. **108**(19), 198103 (2012).
63. E. S. Boyden, F. Zhang, E. Bamberg, G. Nagel, and K. Deisseroth, "Millisecond-timescale, genetically targeted optical control of neural activity," Nat. Neurosci. **8**(9), 1263–1268 (2005).
64. S. S. L. Andersen, A. D. Jackson, and T. Heimburg, "Towards a thermodynamic theory of nerve pulse propagation," Prog. Neurobiol. **88**(2), 104–113 (2009).

1. Introduction

The essential role of neurons is to integrate excitatory and inhibitory synaptic inputs at the level of the neuron soma and dendrites, and transmit this electrochemical information by triggering an action potential(s) (AP) that is propagated along axons to the nerve terminals where the neurotransmitter release activates the second-order neurons [1, 2]. Neuronal relays such as these represent the fundamental units of neuronal networks from the simplest invertebrates to the complex neural circuitry of the human brain. Understanding the basic functions of normal neuronal networks and their disruption in disease states has relied mostly on the recordings of electrical signal [3, 4]. Hence, reliable and accurate recording of

Biomedical Optics EXPRESS

electrical signals has been the cornerstone of understanding the nervous system. Recording electrical signals from single or populations of neurons by electrophysiological techniques has been the mainstay of neuroscience research for the past century [5–7]. Electrophysiological techniques require placement of an electrode in direct contact or close proximity to neurons, presenting inherent technical limitations [8, 9]. These limitations can be a significant hurdle in studies that require long term and high throughput recordings in a network of neurons. Recent developments in multi-electrode array (MEA) electronics platforms have improved throughput and minimized the invasiveness, but remain limited by electrode density and inflexibility of the arrays [10–13].

In response to technical challenges of using standard electrophysiological techniques to monitor neuronal network activity, there have been remarkable advances in the development of fluorescent proteins for optically imaging action potential propagation [14–18]. Recent developments including advanced genetically encoded calcium indicators (GECIs) [19–22], genetically encoded voltage indicators (GEVIs) [23, 24] and voltage sensitive dyes (VSDs) [18, 25, 26] have overcome some of the previous constraints and challenges of optical imaging of membrane potential like low signal-to-noise ratio (SNR), cytotoxicity and slow kinetics [23, 24, 27]. Furthermore, the development of genetically engineered Rhodopsin-fluorescent proteins [28, 29] have revolutionized the characterization of functional neural networks [22, 30]

Label-free optical techniques could provide another alternative to non-invasively record neuronal activities. Unlike electrophysiology, optical interrogation of electrical signaling is achieved indirectly in a contact free manner. Despite the popularity of fluorescence imaging, label-free optical detection of action potential (AP) is highly desirable as it eliminates the need to add exogenous chemical or genetic biosensors with inevitable issues associated with photo-bleaching, photo-toxicity, low SNR and the potential of interfering with normal physiological functions. Endogenous optical changes due to action potential propagation can manifest as changes in scattering [14, 31–33], birefringence [34, 35], refractive index, or optical path length [36–38], which have been studied for the last few decades, beginning in 1950s [16, 17,39–41].

Reported label-free AP studies using optical techniques have been conducted in drosophila CNS [42], giant squid axon [43, 44], lobster [45], and rat-nerve bundle [46, 47] models which typically require averaging of multiple optical signals due to poor signal to noise ratio. In recent years, a number of label free optical techniques [14, 31–38, 42–45] based on phase sensitive interferometry have demonstrated detection of neural activity. High sensitivity in measuring changes in optical path length makes these interferometric techniques particularly attractive for detecting potential AP induced nanoscale changes in neuronal optical properties. While interferometric principle is similar in these techniques, they differ in implementation, neuronal cell/tissue type, and signal detected. To date, none of the label-free optical techniques have successfully demonstrated single shot measurement of individual action potential spikes from single mammalian neurons.

In this article, we report real-time and single shot recording of individual action potentials in a network of cultured mammalian neurons with a label-free optical technique based on phase sensitive low coherence interferometry. Additionally, we propose a plausible framework for the electrical-to-optical signal transduction mechanism that contributes to the measured interferometric signal.

2. Method

2.1. Cortical neuron culture

All experimental procedures were conducted according to UT Arlington Institutional Animal Care and Use Committee approved protocol. Cortical neurons were isolated from 18-day rat embryos after cortical tissues were dissected, cleaned (meningeal layer), enzymatically dissociated (0.125% trypsin in L-15 medium) for 20 minutes at 37 °C. Dissociated cortical

Biomedical Optics EXPRESS

neurons (40,000/ml) were seeded on Poly-D-lysine (PDL, 0.01%, Sigma) pre-coated neuronal cell culture devices. The culture media (Neurobasal medium supplemented B-27 with BDNF and NT-3, 10 ng/ml) in these devices was changed every 24 hours. For patch clamp experiments, neurons were grown in 35 mm glass bottom petri dishes, coated with Poly-D-Lysine and the culture media was changed every 3 days. Glutamate and TTX used for neuronal stimulation and inhibition experiments were purchased from Sigma-Aldrich and Tocris Bioscience, respectively.

2.2. Neuronal cell culture device

Two (25 × 75 × 1 mm) glass slides were used to make each sandwich neuronal cell culture device. First, two holes were drilled (~2 mm diameter) in one glass slide (top slide) using a diamond drill-bit. Water was injected at the drilling point to dissipate heat and avoid glass breakage. Next, the glass slides were thoroughly cleaned using isopropyl alcohol and distilled water. On the top slide, two PDMS wells were attached centered at each hole by plasma bonding to serve as media reservoirs. After applying nontoxic silicone glue on the top surface edges of the bottom glass slide, the top slide was placed on it to fluidically seal the sandwich culture device. The layer of glue in between the glass slides generates a gap of approximately 80 microns. Devices were coated with poly D-lysine 24 hrs prior to cell culturing. Neurons were gently seeded through holes on the sandwich device and the culture media was changed every 24-48 hours to maintain healthy growth of neurons.

2.3. Immunostaining of fixed cortical neuron

Cultured neurons were fixed with 4% paraformaldehyde in phosphate-buffered saline (PBS). Fixed cells were immunostained by standard procedure. Cells were briefly treated with blocking solution that contained 4% goat serum in washing solution (0.5% Triton in PBS) for 1 hour. Mouse anti-β III tubulin monoclonal (mIgG2b, 1:1000; Sigma) primary antibodies were diluted in blocking solution and precooled at 4°C before use. Secondary antibodies Goat anti-mouse IgG2b Alexa Fluor 488 (Green, 1:250; Jackson Immuno Research) were prepared in the washing solution. After blocking, cells were incubated overnight with primary antibodies at 4°C. Next day, cells were washed three times with washing solution followed by incubation with secondary antibody for 1 hour at room temperature and protected from light. Post antibody incubation, cells were washed and stored in PBS solution. Stained cells were imaged using a fluorescence microscope.

2.4. Patch-clamp recording

The patch-clamp set up for computer controlled voltage and current clamp consisted of a recording system, digitizer, and an amplifier (Multiclamp 700B, and Digidata 1440, Molecular Devices). Borosilicate micropipettes of resistance ranging from 3 to 5 MΩ were used for whole-cell patch-clamp. The micropipette was filled with electrolyte solution containing (in mM) 130 K-Gluoconate, 7 KCl, 2 NaCl, 1 $MgCl_2$, 0.4 EGTA, 10 HEPES, 2 ATP-Mg, 0.3 GTP-Tris, and 20 sucrose. The micropipette was mounted on a three-axis motorized micromanipulator (Sutter Instruments). Standard extracellular solution contained (in mM): 150 NaCl, 10 Glucose, 5 KCl, 2 $CaCl_2$, 1 $MgCl_2$ was buffered with 10 mM HEPES (pH 7.3). Recorded neuronal electrical signals were digitized and analyzed (pClamp10 software) to produce AP traces.

2.5. Detection of AP with phase sensitive low coherence interferometry

Optical setup (Fig. 1) used for detection of action potential in a network of cultured cortical neurons consists of a fiber interferometer, high speed spectrometer, and an inverted microscope. Input port of single mode fiber interferometer was seeded with a broadband light source (SLD -Superlum, Inc., λ_c = 860 nm, $\Delta\lambda$ = 63 nm). Light splits at the 2 × 2 fiber coupler and traverses along the output fiber arms. One of the fiber output ports of the interferometer is

Biomedical Optics EXPRESS

attached to the side port of an inverted microscope (Zeiss Axio Observer). The 80/20 beam splitter inside the microscope side port allows for simultaneous cell sample visualization and interferometry. Attached to the side port is a modular opto-mechanical unit which consists of cage system with a fiber connector (FC/APC) and a collimator mounted on a two axis (tip/tilt) mirror mount on one end and a C-mount on the other end that is attached to the microscope side port. Light exiting the single mode fiber is expanded, collimated, and relayed to the microscope objective. Reflected light from the sample is collected by the microscope objective and coupled back to the fiber port. Light incident on the sample (Fig. 1B) is partially reflected from the two reference surfaces of the sandwich neuronal cell culture device. In this common path topology, components of reflected light co-propagate until bottom slide, generating a highly phase stable spectral interference signal (Fig. 1D).

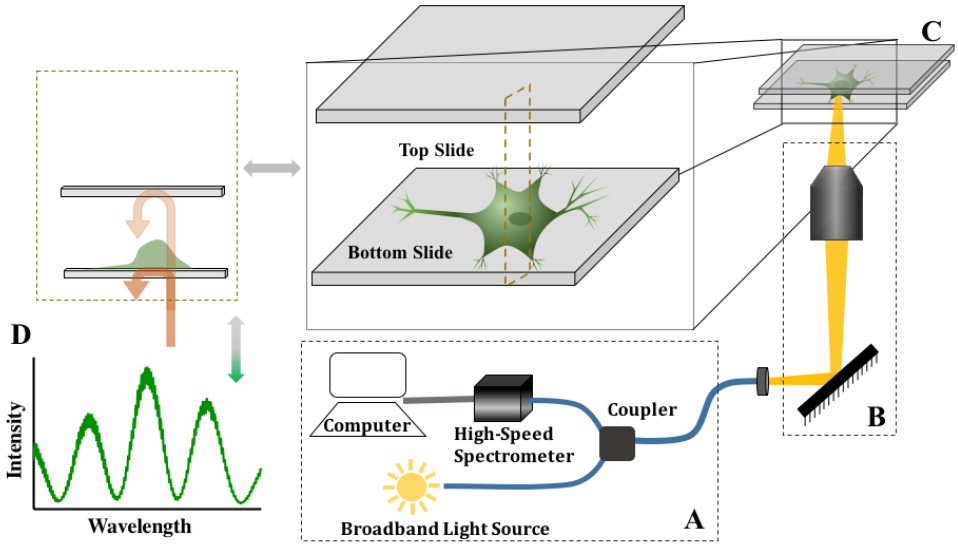

Fig. 1. Optical setup for detecting neuronal activity using low coherence phase sensitive interferometry. (A) Schematic diagram of the interferometric instrument which consists of a broadband source (center wavelength at 860nm, bandwidth of 63 nm), fiber coupler, high-speed spectrometer, and computer with data acquisition system. (B) Output port of the fiber coupler is attached to the side port of an inverted microscope that transmits and focusses light on the s (C) Illustration of neuronal cell culture device in a sandwich configuration consisting of two glass slides that are separated by a fixed gap (~80 μm) with neurons attached to the bottom glass slide, and (D) Light reflecting from the bottom (glass-cell) and the top (cell-media) interfaces of the two glass slides of the neuronal cell culture device couple back into the interferometer and mix to form spectral interference fringe signal.

Choosing two fixed interfaces with comparable reflectivity (glass-cell interface of bottom slide and media-glass of top slide, zoomed inset of Fig. 1(C)) of the neuronal cell culture device generates fringe modulation depth (visibility) close to 100% (Fig. 1(D)) and hence enables highly sensitive measurement of change in optical path difference (OPD). Spectral interference signal generated from light reflecting bottom (glass-cell interface) and top (media-glass interface) of the culture device can be written as [38,49],

$$S_o(k,t) = \alpha S_i(k)\left\{R_1 + R_2 + 2\sqrt{R_1 R_2}\,|\mu(k)|\cos\left[\phi(k,t)\right]\right\} \qquad (1)$$

where, S_i is the spectral density of the broadband light source, α is the coupling efficiency of reflected light from the neuronal cell culture device to the interferometer, and k ($= 1/\lambda$) is the wavenumber. R_1 and R_2 are the reflectivity of the bottom and top interfaces of the cell culture device, respectively. $\mu(k)$ is the spectral coherence function and $\phi(k,t)$ angular phase

Biomedical Optics EXPRESS

difference proportional to the optical path difference (OPD) between top and bottom interfaces of the cell culture device given by the expression [50],

$$\phi(z,t)|_{z=d} = \frac{4\pi}{\lambda_c} p(z,t) = \tan^{-1}\left\{\frac{Im\,S_0(z,t)}{Re\,S_0(z,t)}\right\} \quad (2)$$

where, $p(z,t)$ is the OPD and $S_o(z)$ is the Fourier transform of Eq. (1) calculated at the peak value of the coherence function corresponding to spatial location $z = d$, which is equivalent to the gap of the cell culture device. The spectrometer acquires spectra (depth scans/A-Scans) at maximum rate of ~6000 spectra/s (varies from 4000 to 6000) with a spectral resolution of 0.05 nm. Spectral fringe modulation frequency is proportional to OPD, which is the gap between the two glass (top and bottom) surfaces. Since the physical gap of the neuronal cell culture device remains constant barring any fast thermal and/or mechanical drift in the device or the spectrometer, transient physical changes in the cells will modulate the OPD. Although partially reflected light from other interfaces (top and bottom air-glass interfaces) mix to generate additional interference terms, they are encoded in a different spatial frequency channel and hence do not contribute to calculated phase in Eq. (2).

2.6. Data analysis

A data acquisition card (NI PCIe-8231) and software interface (LabView) was used for data collection. Spectral interferograms are digitized and stored as binary files for post-processing. Each spectral interferogram after *k*-space conversion is Fourier transformed and phase at a spatial frequency channel corresponding to cell culture device gap is calculated as a function of time, $\phi(d,t)$. Temporal phase difference ($\Delta\phi(d,t_n)$) at a given time was calculated by subtracting the measured phase of A-Scan at time t_n from the first (baseline) A-Scan at the start of the experiment. Change in OPD is calculated from the phase difference by,

$$\Delta p(d,t_n) = \frac{\lambda_c}{4\pi}\Delta\phi(d,t_n) = \frac{\lambda_c}{4\pi}\left[\phi(d,t_n) - \phi(d,t_0)\right] \quad (3)$$

For counting and characterizing individual optical pulses, envelope detection (rectification and filtering) and thresholding was done on the measured change in OPD to determine pulse width, peak amplitude, and firing rate. Change in OPD was baselined, filtered and threshold was set above the baseline noise prior to the envelope detection. Second order bandpass Butterworth filter with low pass and high pass cut-off frequencies of 200-300 Hz and 20-30 Hz, respectively, depending on the spectrum acquisition rate (A-Scan), were used to filter the rectified signal. Data was collected in 60 sec segments and only segments that contained optical pulses were considered for feature extraction analysis. Continuous wavelet analysis (Morlet wavelet) was carried out in MATLAB software using 45 ms time windows for time-frequency analysis of optical pulses.

3. Results

Rat cortical neurons were maintained under standard neuronal culture for a period of 14-17 days, over which time they formed an interconnected network of synaptic connection capable of generating self-sustained spontaneous electrical activity. To detect action potential with the interferometric setup, a neuronal cell culture device containing cultured network of cortical neurons (Fig. 2(A)) was firmly mounted on the inverted microscope stage using a custom stage insert, followed by adjustment of microscope objective (10X, N.A = 0.25) focal position to obtain maximum interference fringe signal modulation depth for optimal SNR. Recording experiments were started by first measuring baseline interference signal from a blank region (without any neurons or axons) of the device (Fig. 2(B)) to establish the OPD noise floor. To collect the optical signal from an individual neuron, probe beam was parked on the neuron

Biomedical Optics EXPRESS

soma by laterally translating microscope stage while imaging their relative positions with a camera attached to microscope visualization port. Probe beam (focus spot size ~4.5 μm) covers part of only one cell soma. Interference signal was recorded from a neuron for a period of 3-4 minutes. Next, Glutamate (Glu: 500 μM final concentration) was added into the cell culture device reservoir for stimulation and interference signal was collected. After 10-12 minutes of data collection, Na-channel inhibitor Tetrodotoxin (TTX: 500 nM final concentration) was added to the device and interference signal was collected for a further 6 minutes. Typical temporal changes in OPD observed from these experiments are shown in Fig. 2(C). OPD changes in the form of optical pulses above the baseline are clearly visible in neurons with (+ Glu) and without stimulation. Cultures of cortical rat neurons are well known to form interconnected neuronal networks of excitatory glutaminergic synapses that produce spontaneous random firing in absence of external stimuli. With the addition of exogenous Glutamate, neuronal firing rate increases which is reflected in greater number of transient optical pulses. Effect of TTX, a highly potent sodium ion channel blocker known to effectively kill neuronal firing [51], is clearly noticeable by a reduction in optical pulses. Recorded optical pulses appear to exhibit single or multicyclic oscillations with short to broad temporal widths (Fig. 2(D)). In-depth analysis of the optical pulses and their temporal characteristics are discussed in the subsequent sections.

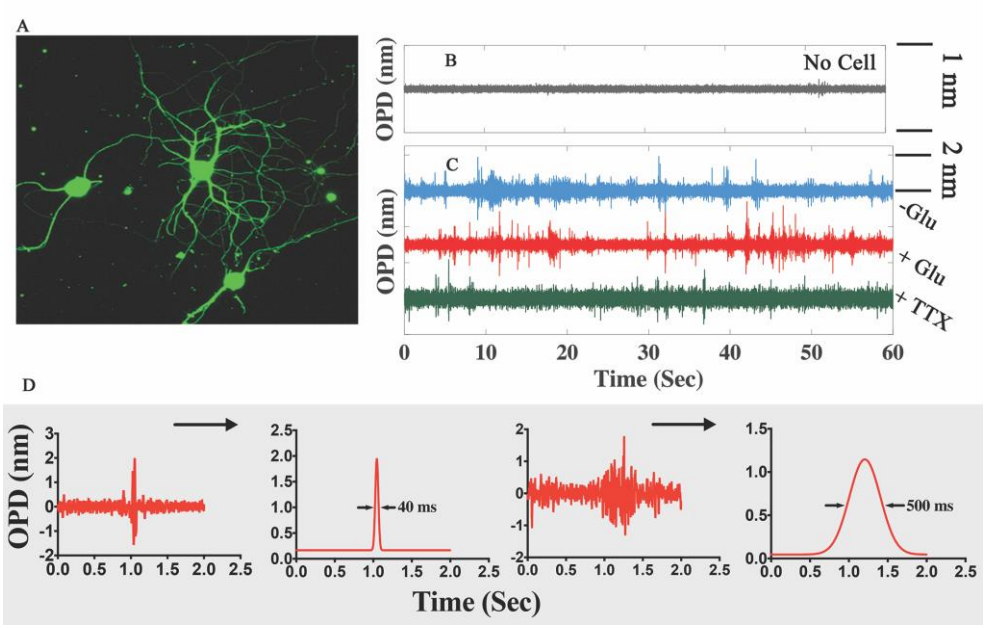

Fig. 2. Representative optical signals recorded from individual neurons in a network. (A) Fluorescence immuno-stained (primary β-III-tubulin antibody- Alexa Fluor 488) image of networked rat cortical neurons used in our experiments. (B) & (C) Temporal change in OPD under different experimental conditions (no cell, cell without any stimulation, cell with Glutamate stimulation, cell with TTX inhibition) showing a non-periodic train of optical signal oscillation from unstimulated and stimulated neurons which die out when inhibited with TTX. Calculated OPD sensitivity (standard deviation of optical trace in (Fig. 2(B))) was 30 pm. (D) Isolated burst of individual optical pulses that have wave packet like signal pulse characteristics and their corresponding envelopes show variation in temporal pulse width.

Electrophysiology studies were carried out on cultured cortical neurons for comparison of the detected optical signal with electrical signal generated during neuronal firing. For each experiment, a single neuron was patched in a network of cultured cortical neurons, and under current clamp of whole cell patch-clamp recording, voltage trace was recorded over time. Spontaneous electrical activity of a networked neuron is reflected in the electrical spikes (Fig.

Biomedical Optics EXPRESS

3(A)) in the absence of exogenous Glutamate stimulation. After few minutes of recording, the same patched cell was stimulated by adding Glutamate in the culture media. Time lapse recording of neuron firing after addition of Glutamate is shown in Fig. 3(A), which clearly shows that Glutamate increases the rate of firing. In another experimental set, patched neuron was subjected to stimulation by Glutamate and subsequently TTX was added to block the sodium ion current. As shown in Fig. 3(B), the TTX diminishes firing activity significantly. The optical results are in close agreement with the electrophysiology recording, where similar outcomes for stimulation and inhibition were observed in the detected optical signal.

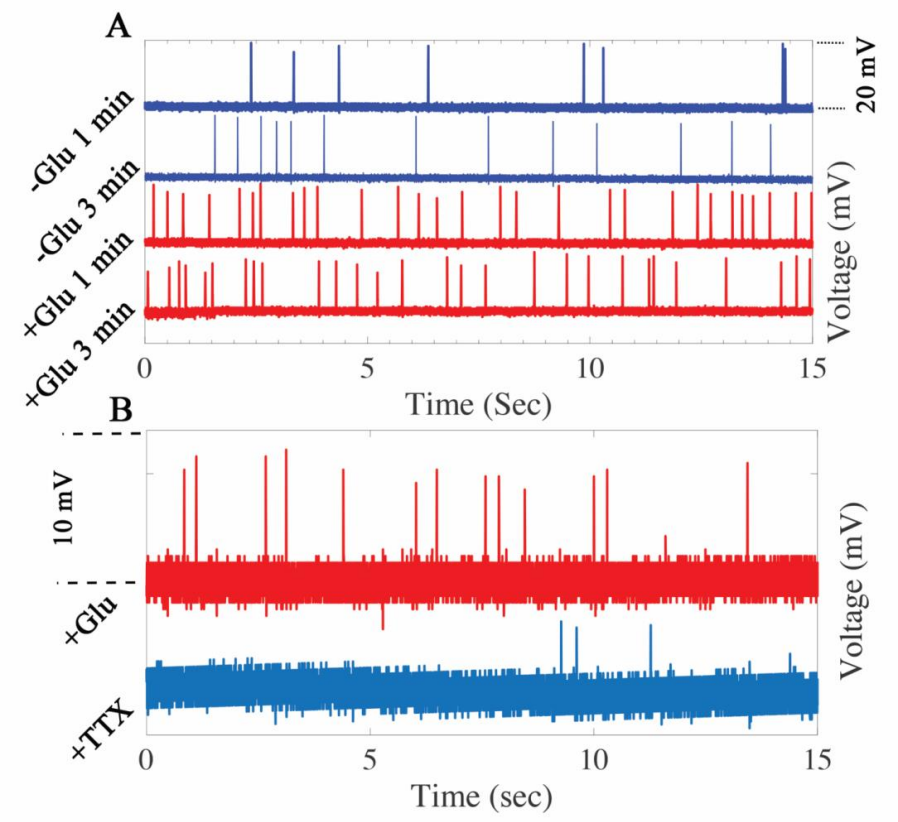

Fig. 3. Patch clamp recording of action potential firing from single neurons. (A) Pre-and post-glutamate stimulation voltage recording (current clamp) of randomly generated action potential spikes in networked neurons. (B) Inhibition of electrical activity with addition of TTX. Recordings in (A) and (B) are from two separate experiments.

Feature extraction analysis of optical pulses was carried out using an envelope detection and thresholding method. Rectified optical signal (Fig. 4(A)) shows a train of optical pulses and each optical pulse envelope can be characterized by its peak magnitude and temporal width. Results summarizing the firing rate (no. of pulses), peak magnitude, and temporal width for unstimulated (-Glu), stimulated (+ Glu), and inhibited (TTX) neurons are shown in Fig. 4(B)-4(D). As expected, the firing rate increases in case of stimulated neurons and diminishes under TTX inhibitions. In the case of TTX administered neurons, few optical pulses were observed, predominantly with short temporal activity window- probably due to the weak, subthreshold firing. In case of spontaneous and stimulated neuronal firing, wider optical temporal period of activity was observed. Wider temporal activity windows are more prominent in the unstimulated neurons, arguably because of the recuperation time availed by the neurons due to lack of aggressive firing. In case of peak amplitudes of the optical pulses, a

Biomedical Optics EXPRESS

wide range of distribution was observed (Fig. 4(D)), which is almost identical in case of stimulated and unstimulated neurons (as Glutamate stimulation only enhances the firing rate, and does not affect the amplitude of action potentials), and close to the baseline in case of TTX inhibition.

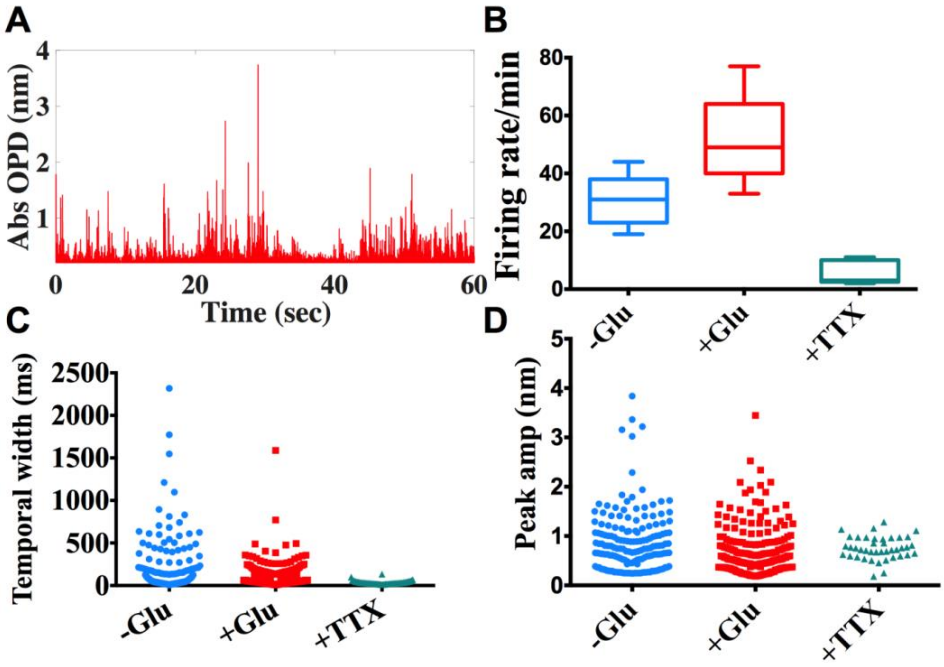

Fig. 4. Analysis of extracted features from individual optical pulse (Fig. 2) (N = 5 neurons). (A) Optical signals are rectified, followed by envelope detection of each pulse. (B) Firing rate of unstimulated vs stimulated/inhibited neurons, ($p<0.05$ for -Glu vs + Glu and -Glu vs + TTX). (C)-(D) scatter plots of envelope width, envelope peak under no stimulation, Glutamate stimulation, and TTX inhibition conditions, respectively.

3.1. Discussion

Detected optical pulses quantify change in OPD, which is a product of physical path length and refractive index. Any modulation of OPD is either due to changes in cell morphology resulting in alterations in cell thickness (height) or refractive index, or a combination of both. Electro-optic effect and dynamic mass redistribution due to depolarization of the cell membrane are potential mechanisms that can modulate cell's refractive index. Modulation in refractive index due to electro-optic effect is expected to temporally follow the AP signal. Electrical activity in the cell membrane is not known to trigger a downstream cellular pathway that could potentially induce cellular mass redistribution resulting in bulk refractive index change. The optical pulses do not follow the AP signal temporally, and hence each optical pulse is a result of change in geometric morphology of the neuronal cell body.

To understand the nature of morphological changes we have analyzed the magnitude, frequency and temporal characteristics (width and shape) of individual optical pulses. Morphological changes can manifest as whole cell deformation (isovolumetric or non-isovolumetric), or fluctuations of the cell membrane. Swelling and contraction have been observed in neurons (nerve fibers, giant squid axons) following action potential, and displacement changes of 0.5-5 nm have been reported [36, 52–54]. While some have proposed underlying cause to be transport of water and ions between the cell and extracellular media [14], others have suggested cation exchange could change the membrane density and generate electrostatic forces in the nerve fibers, creating lateral expansion [55].

Biomedical Optics EXPRESS

Cellular deformation in excitable HEK cells has been studied with interferometry to explore various plausible mechanistic pathways for electromechanical-optical transduction [48]. The study by Oh et al. concluded that direct coupling between membrane potential and membrane tension results in whole cell deformation giving rise to measured change in optical phase signal. No such experimental studies have been reported on mammalian neuron. Membrane displacements can be induced by a transient change in membrane potential, mediated by electromechanical coupling phenomena such as flexoelectricity and piezoelectricity [56]. Previous theoretical [57, 58] and experimental [52, 59] studies using AFM/Electrophysiology have shown that voltage-dependent motions can arise from a fundamental electromechanical coupling between membrane potential and membrane mechanical properties.

We consider the two aforementioned different types of cellular deformation under isovolumetric conditions which can result in membrane displacement: whole cell deformation (in which the dimensional change in cell height is due to change in cell morphology, and is calculated considering the entire cell as one unit with the same refractive index) or localized deformation of the lipid bilayer (only the thickness of lipid membrane changes, and OPD is calculated considering the refractive index of lipid bilayer). Assuming the cell refractive index remains constant, estimated average membrane displacement values are 9 nm and 2.4 nm for whole cell and lipid bilayer deformation cases, respectively. These values are larger in

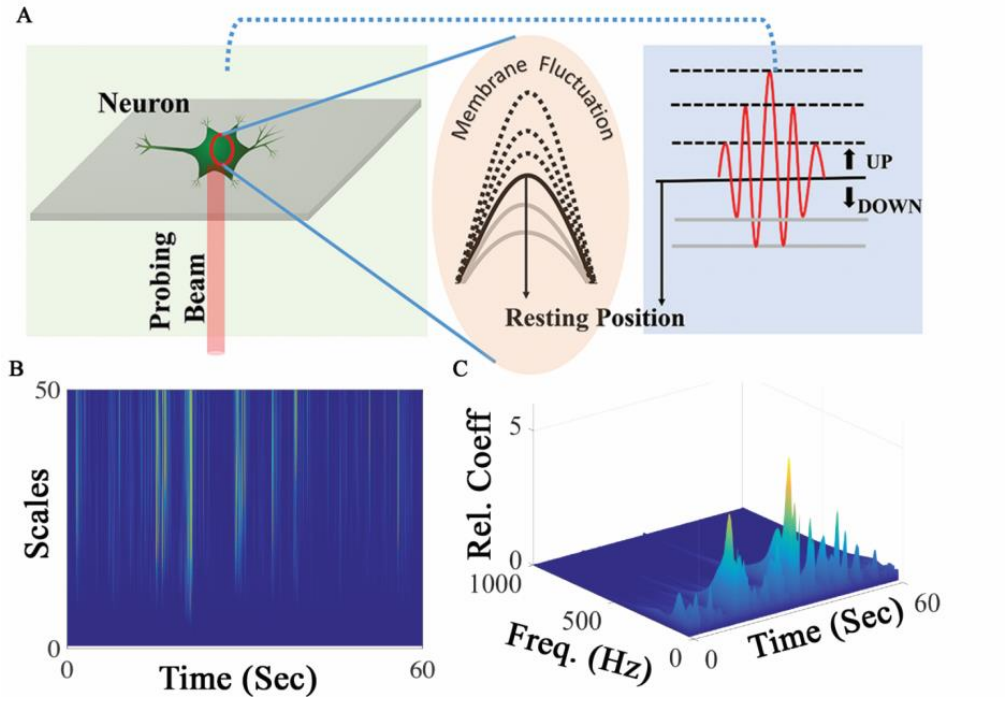

Fig. 5. (A) Illustration of plausible mechanistic origin of optical signal pulse (right panel) due to transient oscillation of neural cell membrane (middle panel) which is triggered by propagating action potential (B) Time-frequency analysis (continuous wavelet transform) of optical pulse train, and (C) Frequency characterization of membrane oscillation from individual optical pulse.

magnitude compared to experimentally measured membrane displacement in giant squid axons, nerve bundles, and HEK cells [48, 52]. Even after considering differences in cell types and inaccuracies in refractive index values due to paucity of experimental data in live cells, our displacement estimates are large. The sandwich geometry of the cell culture device with two references surfaces to generate interference signal can significantly amplify the measured

Biomedical Optics EXPRESS

OPD. Cell membrane deformation, be it local or global, will deflect the membrane plane with respect to the direction of incident light. Even slight membrane deflection can dramatically alter the geometrical path traversed by light and hence the OPD. For example, a 0.5° deflection in membrane plane can change the OPL by ~3 nm, for a cell culture device gap of 80 μm. Considering contribution of amplified OPD due to membrane deflection, estimated membrane displacement in the lipid bilayer are of comparable range to reported values (0.2-5 nm [36, 37, 48, 52, 53, 59]).

Biological membranes can support stationary resonant modes of vibration as well as travelling waves of various forms including surface acoustic waves [5, 60–62]. The top surface (cell-media interface) of the neuronal cell body is a curved membrane under tension that is attached to the bottom (cell-glass interface), and can support 2D Eigen modes of vibration (Fig. 5(A)). Local temperature-dependent nano-mechanical oscillation at characteristic frequencies ranging from 0.8 to 1.6 kHz with amplitudes of 3 nm have been detected in live yeast cells [61]. Standing waves due to whole cell deformation will produce narrow and discrete frequency modes of oscillation. Any other modes besides the fundamental mode of oscillation will wash out the measured OPD change in our measurement setup. Lipid monolayers have shown to support propagating 2D pressure pulses [62]. A recent experimental study has characterized the nature of propagating acoustic waves in lipid monolayers [60]. Depending on the magnitude of excitation, different lateral compressibility regimes of lipid monolayer support propagating pulses of varying timescales and frequencies bandwidths. In the nonlinear compressibility regime, a soliton like pulse propagation with a wide frequency spread (few Hz to 300 Hz) was observed. While in the linear compressibility regime, a transient wave with a reduced amplitude and a narrow frequency distribution travels in the lipid monolayer [60]. Wavelet analysis (Fig. 5(B)) of recorded optical signal shows a wide and continuous frequency bandwidth of membrane vibration in individual optical pulses with a bandwidth of ~200 Hz, centered around 70-100 Hz (Fig. 5(C)). The estimated bandwidth and frequencies are comparable to the reported values in lipid monolayer [60]. We believe that the temporal variation of the optical pulses from the AP signal is due to various combination of factors contributing to the electromechanical coupling.

The electromechanical coupling mechanism is pivotal in dictating the temporal characteristics of the observed optical pulses. Shown in Fig. 6 is the optical recording and zoomed in portions of individual optical pulses of different temporal widths. The shape and timescale of membrane displacement as reflected in the optical pulses are different from the AP signal. Timescale of recorded AP are in the 5-7 ms range, whereas the temporal width of optical pulses ranges from 20 to 300 ms, with an average of 48 ms for 85% of the detected optical pulses. On closer examination of optical pulses shown in Fig. 6(i) and 6(iv), it can be argued that these optical pulses are a collection of single cycle optical pulse shown in Fig. 6(iii), generated by closely bunched APs. Whereas, optical signal in Fig. 6(ii) is a multicyclic pulse, which appears to be a dampened oscillation. Typically, AP signal spikes in a neuronal network exhibit minimal variation in amplitude and temporal width. In our case, for a given electrical input (AP), two different types of mechanical outputs (membrane oscillation) of varying magnitude, shape and time scale are generated. There are two plausible explanations for observed multiple outputs; either the two different types of observed optical pulse are generated due to time varying electrical-to-mechanical coupling efficiency or the multicycle optical pulse is unrelated to AP propagation. It is possible that the membrane supports both, individual single cycle pulses and multicyclic pulses, depending on the mechanical input strength as has been observed in transverse oscillation of lipid monolayer in response to propagating surface wave [60]. The shape and timescales closely resemble the detected optical pulse, which strongly suggests the coexistence of a mechanical surface wave in conjunction with action potential propagation. The strength of electromechanical coupling, mode of membrane vibration, and gap between successive AP firings contribute to the observed oscillatory time-period of optical pulses. In order to tease apart the different kinds of

Biomedical Optics EXPRESS

oscillations, and to determine whether these are in response to a single AP input or a train of AP spikes, future studies will take advantage of optogenetics to analyze the concordance between single and multi-spike trains and the composition of the optical signal [63].

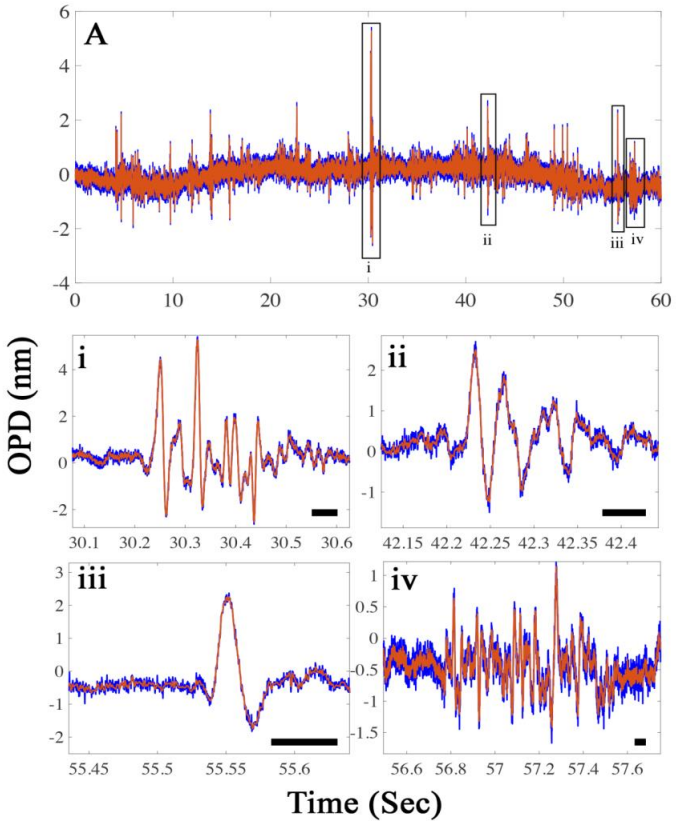

Fig. 6. Optical pulses of varying temporal characteristics (A) Raw (blue) and filtered (low pass-orange) 60 sec extract of optical recording from a signal neuron showing a train of randomly spaced optical pulse. (i-iv) Zoomed section of select windows from optical recordings (A) showing single or multicyclic oscillation of the detected optical pulses. The temporal variation of the selected oscillatory pulses is evident (scale-bar = 50 ms).

Recent theoretical modeling and experimental studies of electromechanical coupling in plasma membrane of axons suggests existence of some form of propagating mechanical wave. Two different theoretical models have examined the input-output relationship in an axonal system. Heimburg et al. have proposed the soliton model for action potential, in which the propagation of action potential ties in with changes in hydrodynamic and thermodynamic properties of the membrane, creating local compression in membrane and forcing the transition from a fluid to gel phase, along with a release of heat, and vice versa [64]. Hady et al. have proposed a model of propagating mechanical action waves in axons triggered by propagation of AP with both lateral and longitudinal displacement of membrane [53]. In the soliton model proposed by Heimburg et al. there is one-to-one correspondence in shape and time scale of electrical and mechanical signals, though it should be noted that in soliton model, entropy driven mechanical pulse propagation induces membrane depolarization and AP propagation. The action wave model predicts membrane displacement that is concomitant to AP in timescale but not in shape. A symmetrical voltage input pulse will result in a single cycle displacement pulse, whose symmetry depends on the relative velocities of AP and

Biomedical Optics EXPRESS

mechanical pulse propagation. Single cycle optical pulses in our experiments look remarkably similar to predictions of the action wave model. It should be noted that the above-mentioned models are based on axons, which are of cylindrical geometry, as opposed to our experiment and analysis on hemispherical neuron soma. Transient oscillatory displacement of the lipid bilayer, frequency and temporal characteristics of oscillations, strongly indicates existence of a propagating surface wave on the neuronal cell membrane triggered by AP.

4. Conclusion

Our interferometry based optical detection method serves as a paradigm for developing an alternative non-invasive tool for studying electrical activity in neuronal systems from a single cell to complex networks. A 2D version of our prototype instrument will significantly increase the throughput by simultaneously recording optical signals from multiple neurons. Implementation of 2D interferometry may be achieved either by raster scanning the probe beam over the sample or acquiring hyperspectral images using a swept broadband source in a microscopy setup. This optical detection technique also benefits from the fact that signals can be selectively collected from specific regions of neuronal circuit, e.g. axon, synaptic junction, dendrite, which is technically challenging using conventional glass microelectrode electrophysiology and thus it can be complementary to electrical recording. 2D interferometry would also be a viable alternative to optical methods using fluorescent imaging sharing advantages such as high throughput, noninvasive and noncontact detection, but without having to resort to averaging, or using high exposure time to mitigate the low SNR of the fluorescent probes. It also eliminates the drawback of using exogenous molecules that may interfere with normal physiological functioning of individual excitable cells and as a consequence, the network properties. The described technique is uniquely suited for in-vitro applications such as screening of neuro-therapeutic drugs, studying functional recovery of injured neurons and disrupted neuronal networks, and influence of electrical and magnetic field on neuronal activity. Moreover, rather than an epiphenomenon, recent studies have raised the intriguing possibility of a potential coupling between propagating mechanical wave and AP. Mechanical wave energy could feedback into the propagating AP in a coupled electromechanical system. Our label-free interferometric technique will be a uniquely suited for studying fundamental mechanism of electromechanical coupling and its implications in transmission of signals in neuronal networks.

Funding

National Institutes of Health (NIH) (NS084311) and Provost's office (University of Texas at Arlington).

Acknowledgment

The authors would like to thank Saurabh Kokane (UTA) for fabricating micro pipettes used in patch-clamp experiments.

Disclosures

The authors declare that there are no conflicts of interest related to this article.